varies on the edge of the pile and is thicker and not as extreme in velocity reduction as observed in some regions (*42*). The *S*-velocity reductions are comparable to the *P*-velocity reductions (*27*) in this ULVZ. This finding indicates that little or no partial melt accumulated under this edge of the pile, whereas strong ULVZs with partial melting are found on other margins (*43*).

Thermal modeling gives direct determinations of thermal gradients for the CMB region. Regional heat flux into the base of the LLSVP is 85 ± 25 mW/m^2, close to average surface heat flux, for $K = 10$ W/(m·K). Global extrapolation suggests a lower bound on CMB heat flow of 13 ± 4 TW, subject to large uncertainty in K. These relatively high values favor the sequestration of heat-producing radiogenic elements in the core and a relatively young age for the inner core.

References and Notes

1. Q. Williams, in *The Core-Mantle Boundary*, M. Gurnis, M. E. Wysession, E. Knittle, B. A. Buffett, Eds. (American Geophysical Union, Washington, DC, 1998), pp. 73–81.
2. M. Murakami, K. Hirose, K. Kawamura, N. Sata, Y. Ohishi, *Science* **304**, 855 (2004).
3. A. R. Oganov, S. Ono, *Nature* **430**, 445 (2004).
4. T. Lay, E. J. Garnero, in *The State of the Planet, Frontiers and Challenges in Geophysics*, R. S. J. Sparks, C. J. Hawkesworth, Eds. (American Geophysical Union, Washington, DC, 2004), pp. 25–41.
5. J. Wookey, S. Stackhouse, J.-M. Kendall, J. Brodholt, G. D. Price, *Nature* **438**, 1004 (2005).
6. T. Iitaka, K. Hirose, K. Kawamura, M. Murakami, *Nature* **430**, 442 (2004).
7. T. Tsuchiya, J. Tsuchiya, K. Umemoto, R. M. Wetzcovitch, *Geophys. Res. Lett.* **31**, L14603 (2004).
8. K. Hirose, R. Sinmyo, N. Sata, Y. Ohishi, *Geophys. Res. Lett.* **33**, L01310 (2006).
9. S. Ono, A. R. Oganov, *Earth Planet. Sci. Lett.* **236**, 914 (2005).
10. T. Tsuchiya, J. Tsuchiya, K. Umemoto, R. M. Wentzcovitch, *Earth Planet. Sci. Lett.* **224**, 241 (2004).
11. W. L. Mao *et al.*, *Proc. Natl. Acad. Sci. U.S.A.* **101**, 15867 (2004).
12. Y. Kobayashi *et al.*, *Geophys. Res. Lett.* **32**, L19301 (2005).
13. S. Stackhouse, J. P. Brodholt, G. D. Price, *Geophys. Res. Lett.* **33**, L01304 (2006).
14. J.-F. Lin *et al.*, *Nature* **436**, 377 (2005).
15. S. Akber-Knutson, G. Steinle-Neumann, P. D. Asimow, *Geophys. Res. Lett.* **32**, L14303 (2005).
16. R. Caracas, R. E. Cohen, *Geophys. Res. Lett.* **32**, L16310 (2005).
17. A. R. Oganov, S. Ono, *Proc. Natl. Acad. Sci. U.S.A.* **102**, 10828 (2005).
18. S. Tateno, K. Hirose, N. Sata, Y. Ohishi, *Geophys. Res. Lett.* **32**, L15306 (2005).
19. J. W. Hernlund, C. Thomas, P. J. Tackley, *Nature* **434**, 882 (2005).
20. C. Thomas, E. J. Garnero, T. Lay, *J. Geophys. Res.* **109**, B08307 (2004).
21. C. Thomas, J.-M. Kendall, J. Lowman, *Earth Planet. Sci. Lett.* **225**, 105 (2004).
22. A. Hutko, T. Lay, E. J. Garnero, J. Revenaugh, *Nature* **441**, 333 (2006).
23. C. Flores, T. Lay, *Geophys. Res. Lett.* **32**, L24305 (2005).
24. M. Avants, T. Lay, S. A. Russell, E. J. Garnero, *J. Geophys. Res.* **111**, B05305 (2006).
25. M. Avants, T. Lay, E. J. Garnero, *Geophys. Res. Lett.* **33**, L07314 (2006).
26. S. P. Grand, *Philos. Trans. R. Soc. London Ser. B* **360**, 475 (2002).
27. S. A. Russell, C. Reasoner, T. Lay, J. Revenaugh, *Geophys. Res. Lett.* **28**, 2281 (2001).
28. S.-N. Luo, S. Ni, D. V. Helmberger, *Earth Planet. Sci. Lett.* **189**, 155 (2001).
29. A. To, B. Romanowicz, Y. Capdeville, N. Takeuchi, *Earth Planet. Sci. Lett.* **233**, 137 (2005).
30. S. Ni, D. V. Helmberger, J. Tromp, *Geophys. J. Int.* **161**, 283 (2005).
31. S. A. Russell, T. Lay, E. J. Garnero, *J. Geophys. Res.* **104**, 13183 (1999).
32. K. Hirose, *Rev. Geophys.* **44**, RG3001 (2006).
33. F. Stacey, *Physics of the Earth* (Brookfield, Brisbane, Australia, ed. 3, 1992).
34. H. N. Pollack, S. J. Hurter, J. R. Johnson, *Rev. Geophys.* **31**, 267 (1993).
35. C. Lithgow-Bertelloni, M. A. Richards, *Rev. Geophys.* **36**, 27 (1998).
36. I. Sidorin, M. Gurnis, D. V. Helmberger, *Science* **286**, 1326 (1999).
37. J. Trampert, F. Deschamps, J. Resovsky, D. Yuen, *Science* **306**, 853 (2004).
38. M. Ishii, J. Tromp, *Science* **285**, 1231 (1999).
39. K. Hirose, N. Takafuji, N. Sata, Y. Ohishi, *Earth Planet. Sci. Lett.* **237**, 239 (2005).
40. A. K. McNamara, S. Zhong, *Nature* **437**, 1136 (2005).
41. D. Sun, T.-R. A. Song, D. Helmberger, *Geophys. Res. Lett.* **33**, L12S07 (2006).
42. S. Rost, E. J. Garnero, Q. Williams, M. Manga, *Nature* **435**, 666 (2005).
43. M. Thorne, E. J. Garnero, *J. Geophys. Res.* **109**, B08301 (2004).

44. We thank Q. Williams, K. Hirose, J. Brodholt, and the anonymous reviewers for helpful discussion and comments. We also thank H. Igel and G. Jahnke for help with the 2.5D SHaxi code. This work was supported in part by NSF under grants EAR-0125595, EAR-0453884, and EAR-0453944 and by the French Ministry of Research. Seismic data were obtained from the Incorporated Research Institutions for Seismology, the University of California at Berkeley, and California Institute of Technology/U.S. Geological Survey TRInet data centers. The Arctic Region Supercomputing Center at the University of Alaska at Fairbanks provided computer time.

Supporting Online Material

www.sciencemag.org/cgi/content/full/314/5803/1272/DC1
SOM Text S1 and S2
Figs. S1 to S17
References

1 August 2006; accepted 4 October 2006
10.1126/science.1133280

REPORTS

Radar Imaging of Binary Near-Earth Asteroid (66391) 1999 KW4

Steven. J. Ostro,[1]* Jean-Luc Margot,[2] Lance A. M. Benner,[1] Jon D. Giorgini,[1] Daniel J. Scheeres,[3] Eugene G. Fahnestock,[3] Stephen B. Broschart,[3] Julie Bellerose,[3] Michael C. Nolan,[4] Christopher Magri,[5] Petr Pravec,[6] Petr Scheirich,[6] Randy Rose,[1] Raymond F. Jurgens,[1] Eric M. De Jong,[1] Shigeru Suzuki[1]

High-resolution radar images reveal near-Earth asteroid (66391) 1999 KW4 to be a binary system. The ~1.5-kilometer-diameter primary (Alpha) is an unconsolidated gravitational aggregate with a spin period ~2.8 hours, bulk density ~2 grams per cubic centimeter, porosity ~50%, and an oblate shape dominated by an equatorial ridge at the object's potential-energy minimum. The ~0.5-kilometer secondary (Beta) is elongated and probably is denser than Alpha. Its average orbit about Alpha is circular with a radius ~2.5 kilometers and period ~17.4 hours, and its average rotation is synchronous with the long axis pointed toward Alpha, but librational departures from that orientation are evident. Exotic physical and dynamical properties may be common among near-Earth binaries.

The swarm of near-Earth asteroids (NEAs) whose orbits pass close to that of Earth contains about a thousand objects with effective diameters as large as 1 km. Some 840 of these large NEAs have been discovered, and 28 of them have been found by radar and/or photometry to be binary systems (*1*, *2*), which potentially can offer unique insights into NEA origin and evolution. However, detailed information about the physical configurations and dynamical states of NEA binaries is lacking. Here we present decameter-resolution radar images and a detailed model of one of the largest binary NEAs, (66391) 1999 KW4.

KW4 is one of several dozen NEAs whose orbits cross those of Earth, Venus, and Mercury. The asteroid's May 2001 approach to within 0.032 astronomical units (AUs) from Earth was its closest until 2036, and we conducted extended observations using the Goldstone X-band (8560-MHz, 3.5-cm) and Arecibo S-band (2380-MHz, 13-cm) radar systems (table S1). Goldstone is more fully steerable than Arecibo,

[1]Jet Propulsion Laboratory, California Institute of Technology, Pasadena, CA 91109–8099, USA. [2]Department of Astronomy, Space Sciences Building, Cornell University, Ithaca, NY 14853–6801, USA. [3]Department of Aerospace Engineering, University of Michigan, 1320 Beal Avenue, Ann Arbor, MI 48109–2140, USA. [4]Arecibo Observatory, HC3 Box 53995, Arecibo, PR 00612, USA. [5]University of Maine at Farmington, 173 High Street–Preble Hall, Farmington, ME 04938, USA. [6]Astronomical Institute, Academy of Sciences of the Czech Republic, Fričova 1, CZ-25165 Ondřejov, Czech Republic.

*To whom correspondence should be addressed. E-mail: ostro@reason.jpl.nasa.gov

so the Goldstone image sequences provided our longest continuous coverage (spanning 21 to 29 May, with image sequences up to 6.5 hours long), whereas the Arecibo echoes are an order of magnitude stronger. We also obtained weak, but useful, Arecibo echoes during the asteroid's 0.13-AU approach in June 2002. Our observations used periodic binary phase–coded waveforms to obtain images of the distribution of echo power in time delay (range) and Doppler frequency (line-of-sight velocity) (*3*, *4*). Each of our 279 Arecibo images and 1075 Goldstone images reveal two distinctly separated components (we call the larger one Alpha and the smaller one Beta) and provide excellent orbital phase coverage (Fig. 1).

Alpha's echo bandwidths increased from 21 May to a maximum on 25 May and then decreased through 29 May, indicating that our view was closer to equatorial in the middle of the 9-day experiment. In the Arecibo single-date time exposures (Fig. 1), the 26 May image shows a trailing edge where the echo bandwidth reaches a maximum, but during the next 3 days, as our view migrates away from the equator, we see echoes from increasingly beyond that maximum-bandwidth delay, with the bandwidth of those echoes decreasing. This is the progression one would expect for a flattened (oblate) spheroidal target. Alpha's echo edge frequencies vary by only a few percent during the object's several-hour rotation, indicating a nearly circular pole-on silhouette. Analysis of the day-to-day sequence of Alpha's bandwidths constrains the ecliptic (longitude, latitude) of the object's pole direction to be within 20° of either (150°, 60°) or (330°, −60°). A search for sidereal periods P_A consistent with the reappearance times of feature orientations in images on successive days eliminates the first possibility and constrains P_A to be near 2.765 hours. In images showing the components with their trailing edges at similar ranges [and hence their centers of mass (COMs) presumably at approximately similar ranges], the 21 to 29 May variation in the bandwidth from the middle of Alpha to the middle of Beta increases, peaks, and decreases in a manner commensurate with the pattern for Alpha's bandwidth, suggesting that Alpha's equatorial plane and the system's orbit plane are approximately coplanar. When the components are aligned in Doppler frequency or range, Beta's signature is very symmetrical, with the approaching and receding limbs extending to similar delays. However, away from the conjunctions, Beta's limbs extend to distinctly different ranges, with the pattern as expected if the object is at least slightly elongated and if its longest dimension points toward Alpha (fig. S1).

Although a single radar image can be geometrically ambiguous, the delay-Doppler trajectory of any point on the surface of a rotating rigid body is unique if the radar is not in the target's equatorial plane. Therefore (*5*), with a time series of images providing enough echo

Fig. 1. Single-date, multi-run sums. Sums of delay-Doppler radar images obtained with Arecibo (**left**) and Goldstone (**right**) on each observation date. These sums are long time exposures (table S1) that show the orbital phase coverage of the secondary component (Beta) in each observing sequence. The pairs of Arecibo time exposures on 26 to 28 May correspond to radar setups with slightly different Doppler frequency resolutions (table S1). The radar is toward the top, rotation and orbital motion are counterclockwise, and each image has a height of 5625 m (37.5 μs of roundtrip time delay) and 117.2 cm s^{-1} of line-of-sight velocity (Doppler frequency of 18.6 Hz at Arecibo's 2380-MHz transmitter frequency or 66.9 Hz at Goldstone's 8560-MHz frequency). Vertical smear of the primary component (Alpha) due to motion about the system barycenter is evident in the long Goldstone exposures.

Table 1. Relative orbit of Beta about Alpha. Least-squares estimates of the elements of the average 2001–2002 relative orbit are given in the J2000 equatorial frame along with their standard errors and correlation matrix. The epoch, *T*, which corresponds to calendar date 26 May 2001 09:55:00.5, represents the time at which Beta is at pericenter. Ω and *i* correspond to a pole direction at right ascension = 15.4° ± 3° and declination = −66.1° ± 2°. Our estimate of P_{Orbit} from Beta-Alpha delay-Doppler differences, 1045.34 ± 2.16 min, is marginally compatible with our estimate of P_{Orbit}, 1048.18 ± 1.15 min, from modeling of mutual events observed in optical lightcurves during 3 to 12 June 2001 (*2*) with the orbital pole fixed at the radar estimate (*26*). [A decrease in the number of revolutions of Beta around Alpha by one between the 2001 and 2002 epochs of the radar measurements corresponds to an increase in orbital period of 2.04 min. There are solutions that fit the radar data with an orbital period of 1047.38 min, but not without a statistically unacceptable increase (25%) in the chi-square value.] MJD, modified Julian date; arg. peri., argument of perihelion.

Parameter	Estimate	P_{ORBIT}	*a*	*T*	Ω	*i*	ω	*e*
P_{Orbit} [period (hours)]	17.4223 ± 0.036	1.00	−0.05	−0.02	−0.02	−0.06	−0.02	0.06
a [semimajor axis (*m*)]	2548 ± 15	−0.05	1.00	0.24	0.52	0.45	0.24	−0.12
T (epoch, MJD)	52055.4132 ± 0.88	−0.02	0.24	1.00	0.18	0.58	1.00	−0.53
Ω [long. asc. node (°)]	105.4 ± 3	−0.02	0.52	0.18	1.00	−0.07	0.18	0.07
i [inclination (°)]	156.1 ± 2	−0.06	0.45	0.58	−0.07	1.00	0.58	−0.30
ω [arg. peri. (°)]	319.7 ± 182	−0.02	0.24	1.00	0.18	0.58	1.00	−0.53
e (eccentricity)	0.0004 ± 0.0019	0.06	−0.12	−0.53	0.07	−0.30	−0.53	1.00
M (total mass)	(2.488 ± 0.054) × 10^{12} kg							

strength, resolution, and orientational coverage, one can estimate the target's three-dimensional shape, spin state, and radar scattering properties, along with the location of the COM in each delay-Doppler frame.

For each component, our shape estimation used images vignetted to exclude the other component. We summed independent images, attempting to strike a balance between maximizing signal-to-noise ratio and minimizing rotational and translational smear (table S1). The latitude-longitude coverage of the image sets used in the modeling is excellent (fig. S2). Our strategy was to start with an ellipsoid model and proceed first to a model in which surface displacement is expressed as a spherical harmonic series and then proceed to a vertex model, in each case adjusting the free parameters to optimize the resemblance between images synthesized from the shape model and the radar images (*3*, *4*). Ellipsoid models, "harmonic" models, and vertex models were realized as polyhedra with triangular sides.

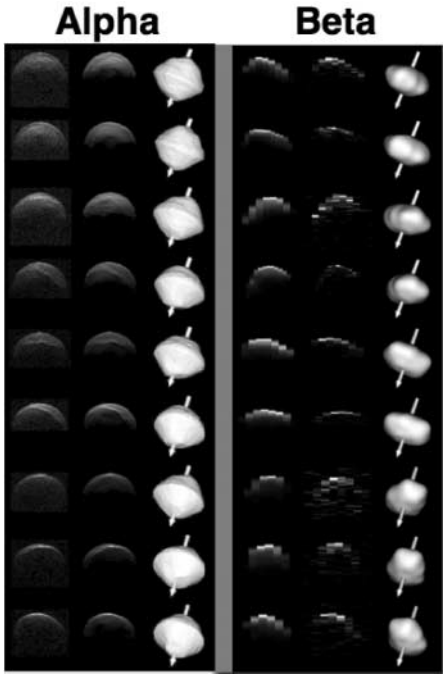

Fig. 2. Examples of images and fit results. Each three-frame horizontal collage shows an Arecibo radar image used in the estimations, the corresponding image synthesized from the shape model, and a plane-of-sky (POS) view of that model. Each three-frame collage consists of three squares with 2.0-km sides for Alpha and 0.8-km sides for Beta. In the delay-Doppler images, the radar is toward the top and the object rotates counterclockwise. In the POS frames, north is toward the top and the arrow represents the spin vector. The Alpha collages (**left**) show images obtained on (top to bottom) 26, 26, 27, 27, 27, 28, 28, 29, and 29 May. The Beta collages (**right**) show images obtained on 26, 26, 27, 27, 28, 28, 29, 29, and 29 May. See (*29*) for tabulation of all images used in the shape modeling and corresponding three-frame collages.

[A triangular polyhedron with V vertices has $(2V-4)$ faces and $(3V-6)$ edges. Larger values of V provide greater spatial resolution and, for ellipsoid and harmonic models, sample the mathematical function more densely, but they also slow the estimation.] We used enough vertices to accommodate the most detailed structure revealed in the data (Fig. 2).

To model the components' motion with respect to each other (*1*), we assumed a Keplerian (two-body, point-mass) orbit of Beta's COM with respect to Alpha's COM and used least squares to estimate the orbit elements from the delay and Doppler offsets of Beta's COM from Alpha's COM as determined in the shape reconstructions. Conservative uncertainties, on the order of several times the image resolution, were assigned to the Beta-Alpha offsets. The best-fit solution [postfit root mean square (rms) residuals of 30 m and 0.75 cm s^{-1} (Table 1)] yields an orbital period $P_{Orbit} = 17.4223 \pm 0.036$ hours and a semimajor axis $a = 2548 \pm 15$ m, with the pole at ecliptic (longitude, latitude) = (326°, −62°) ± 5°. P_{Orbit} and a constrain the system's total mass M by Kepler's third law and yield $M = (2.488 \pm 0.054) \times 10^{12}$ kg (*6*).

The distances R_A and R_B of the components' COMs from the binary system's barycenter are related to the component masses M_A and M_B by $R_B/R_A = M_A/M_B$. Thus, any candidate mass ratio defines the delay-Doppler location of the barycenter with respect to those of the components' COMs in any given image, and hence yields estimates of the time-delay and Doppler frequency of hypothetical echoes from the barycenter at the receive-time epoch of the image. We estimated the heliocentric orbit of the asteroid in the absolute reference frame of the planetary ephemerides (table S2), using radar and optical astrometry and evaluating the goodness of fit as a function of M_A/M_B. Fits to optical and Goldstone astrometry (*7*) (table S3) show a sharp chi-square minimum at $M_A/M_B = 17.4 \pm 2.5$ (fig. S3), which with the results in Table 1 yields the component masses in Table 2, as well as a value for the radius of Alpha's orbit about the barycenter: $R_A = 138 \pm 22$ m.

Alpha's shape (Fig. 3 and fig. S4) is distinguished by a prominent equatorial bulge whose several-hundred-meter vertical extent is defined in the north by a continuous, very abrupt ridge and in the south by more subtle, discontinuous gradations. Much of the surface appears to have subtle structure with perhaps a few decameters of vertical relief. Some concavities might be interpreted as ~100-m impact craters, but most of the structure looks nondescript.

Alpha's bulk density, 1.97 ± 0.24 g cm^{-3}, and rotation period, $P_A = 2.7645 \pm 0.0003$ hours, reveal this object to be in a highly unusual physical state. Alpha spins fast enough so that the "potential low" of the body is located at its equator. That is, particles allowed to freely move across the surface of Alpha would naturally seek out the equator as the lowest-energy

Table 2. Alpha and Beta model characteristics. The Alpha model has 4586 vertices and 9168 facets, with a mean edge length of 39 m and effective angular resolution of 3°. The Beta model is a spherical harmonics representation of degree and order 8 realized with 1148 vertices and 2292 facets, with a mean edge length of 26 m and an effective angular resolution of 7°. The positive side of Alpha's longest principal axis (+x) is on the plane of the sky and approaching Earth on 25 May 2001 at 12:23:21. We assumed uniform internal density and principal-axis rotation about the z axis. The dynamically equivalent equal-volume ellipsoid (DEEVE) is the homogeneous ellipsoid having the same moment-of-inertia ratios and volume as the model. The assigned standard errors include our assessment of systematic effects. The uncertainties in the components' individual masses include contributions from the uncertainty in the system's total mass (Table 1) and from the uncertainty in the determination of the mass ratio. Uncertainties in densities and other ratios are calculated with Fieller's theorem (*27*, *28*). Our value for Alpha's spin period agrees with the value, 2.7650 ± 0.0004 hours, derived from lightcurves by (*2*). Digital versions of the models in Wavefront format are available (*29*).

		Alpha	Beta
Extents along principal axes (km):	x	1.532 ± 3%	0.571 ± 6%
	y	1.495 ± 3%	0.463 ± 6%
	z	1.347 ± 3%	0.349 ± 6%
Area (km^2)		5.744 ± 6%	0.674 ± 12%
Volume (km^3)		1.195 ± 9%	0.048 ± 18%
Mass (10^{12} kg)		2.353 ± 0.100	0.135 ± 0.024
Density (g cm^{-3})		1.97 ± 0.24	2.81 (+0.82, −0.63)
Moment of inertia ratios:	I_z/I_x	1.187 ± 5%	1.74 ± 10%
	I_y/I_x	1.133 ± 5%	1.18 ± 10%
Equivalent diameter (km) of a sphere with the model's volume		1.317 ± 3%	0.451 ± 6%
DEEVE extents (km):	x	1.417 ± 3%	0.595 ± 6%
	y	1.361 ± 3%	0.450 ± 6%
	z	1.183 ± 3%	0.343 ± 6%
Rotation period (hours)		2.7645 ± 0.0003	17.4223 assumed
Pole direction [ecliptic long., lat. (°)]		(326, −65) ± 3	(326, −62) assumed

state (Fig. 3). The equatorial band has a very wide variation in slope, due mostly to the total acceleration of particles on the equatorial band being almost zero, but inward. Thus, in the equatorial region, particles are deposited on the surface in a nearly weightless environment and currently are being retained very tenuously. If Alpha's spin were any faster, loose regolith at certain distinct equilibrium points (*8*) would be placed in orbit about Alpha and would eventually reimpact Alpha at some other location. The existence of these equilibrium points just at the surface places the system exactly at the boundary of what a rotating body could sustain.

Alpha's radar polarization ratio, SC/OC = 0.45 ± 0.10, indicates more severe decimeter-scale near-surface roughness than on "typical" radar-detected NEAs like 25143 Itokawa and 433 Eros, but specular glints at the leading edges of the images (Fig. 2) show that the surface also possesses a very smooth component. Our modeling used a hybrid, two-term scattering law to accommodate both specular and diffuse scattering, and the parameter values estimated for the specular term correspond to a very shallow rms slope with respect to the model's facets and a near-surface bulk density between 0.6 and 1.2 g cm^{-3}, as might be expected for tenuously held regolith of stony meteoritic material.

The grain density of plausible meteorite matches to the asteroid's S spectral class (*9*) ranges from about 3.7 g cm^{-3} for ordinary chondrites (*10*) to about 5.1 g cm^{-3} for stony irons (*11*). Thus, Alpha's porosity probably is between 40 and 66%, comparable to values for lunar regolith core samples. Our value for Alpha's density is comparable to or lower than other (spacecraft-derived) values for S-class asteroids: 1.95 ± 0.14 g cm^{-3} for the 0.4-km NEA Itokawa (*12*), 2.67 ± 0.03 g cm^{-3} for the 17-km NEA Eros (*13*), and 2.6 ± 0.5 g cm^{-3} for the 28-km main-belt asteroid 243 Ida (*14*). Alpha's porosity apparently exceeds that of the latter two objects but is similar to those of Itokawa and the 58-km C-class main-belt asteroid 253 Mathilde (*15*) and several other C-class objects (*16*).

Together, Alpha's size, shape, spin, density, and porosity reveal it to be an unconsolidated gravitational aggregate close to its breakup spin rate, suggesting that KW4's origin involved spin-up and disruptive mass shedding of a loosely bound precursor object (*1*, *2*). The disruption may have been caused by tidal effects of a close encounter with a planet (*17*–*20*) or by torques due to anisotropic thermal radiation of absorbed sunlight (the YORP effect) (*21*). The near-circularity of Alpha's pole-on profile further suggests that the disruption may have produced a quasi-circular disk of particles rather than merely a prolate elongated body (*22*).

Our Beta shape model (Fig. 3 and fig. S4) is about one-third the size of Alpha and more elongated, flattened, and asymmetrical. Our Beta density estimate, 2.81 (+0.82, −0.63) g cm^{-3}, is about 43% larger than our value for Alpha, presumably due to some combination of Beta's different spin, the circumstances of Beta's formation, and the dynamical and collisional evolution of the KW4 system (*22*). Beta's disk-integrated radar properties are indistinguishable from Alpha's. Analysis of dual-polarization images reveal a drop in the SC/OC ratio toward Beta's leading edge, suggesting the presence of smooth and rough surface components, as with Alpha. Beta's density allows porosities up to 42% if it resembles ordinary chondrites and from 29 to 58% if it resembles stony irons.

Whereas reconstruction of Alpha was very robust, with Beta our estimations were consistent with rotation periods between 17.3 and 17.5 hours but could not discriminate between specific values in that interval. Moreover, values for Beta's rotation period within the range spanned by the May radar and June optical estimates of P_{Orbit} (Table 1) led to indistinguishable harmonic models for which synthesized images fit the boundaries of the delay-Doppler echo distributions but could not fit image fine structure as well as with Alpha. Vertex models were unable to improve upon the image fits; relaxing the requirement of principal-axis rotation did not help. For certain "conjunction epochs" (with both components' COMs at either the same range or the same Doppler), solutions with any candidate period placed Beta's long axis at least several degrees from the Alpha-Beta line. Experiments in which only short subsets of images were centered on those epochs instead of the full Beta data set yielded smaller angular offsets but still are suggestive of Beta's rotation not being exactly synchronous. These results are at odds with our shape modeling assumption of unforced free rotation and suggest that Beta may exhibit sizable librations in longitude.

The dynamics of the KW4 system have unforeseen complexity (*22*), potentially involving variations in the orbit and Beta's spin state on a variety of time scales due to dynamical excitation from several possible sources. Consequently, our orbit (Table 1) and rotation parameters (Table 2) represent averages corresponding to the geometrical configurations sampled by the radar observations. The gross dimensions and periodicities of the KW4 system are typical of NEA binaries (*2*), so many of them may share KW4's physical and dynamical complexity.

Over time scales of tens of thousands of years, variations in KW4's heliocentric orbit due to planetary perturbations produce configurations with ecliptic crossings near the orbits of Mercury, Venus, or Earth. [The eccentricity varies from

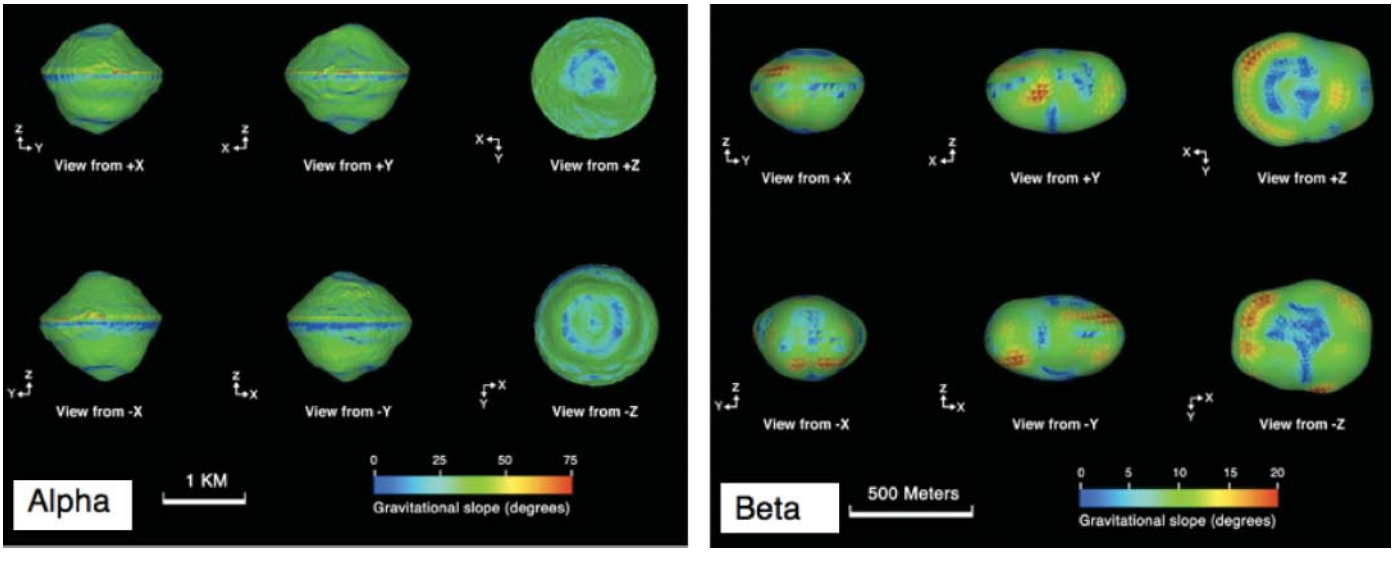

Fig. 3. Principal-axis views of the Alpha (**left**) and Beta (**right**) shape models. Colors indicate effective gravitational slope (the angular deviation from the local downward normal of the total acceleration vector due to gravity and rotation), calculated with the model densities (Table 2). Alpha's slopes average 28° with a maximum of 70°, whereas Beta's average 9° with a maximum of 18°. Beta's +*x* axis points toward Alpha.

0.68 to 0.81 and the inclination varies from 39° to 14° (*23*, *24*)]. Thus, the KW4 binary system could have originated in a close flyby past any of those planets. Currently, KW4's orbit is close to the (e = 0.68, i = 39°), state and the ascending node is very close to Earth's semimajor axis. Within the nearly two-millennium window (1179 to 2946) of accurate close-approach prediction (table S4) allowed by available radar plus optical astrometry, KW4 makes 186 close Earth approaches and no approaches to any other planet. With Alpha's current pole direction assumed, the sub-Earth latitude at closest approach is generally equatorial, with mean and rms of $-7° \pm 20°$. This geometric configuration conceivably could be the signature of an extremely recent Earth-flyby origin of the system.

References and Notes

1. J. L. Margot *et al.*, *Science* **296**, 1445 (2002).
2. P. Pravec *et al.*, *Icarus* **181**, 63 (2006).
3. Our observational, data reduction, and shape-estimation techniques were nearly identical to those described in reference to asteroid 1580 Betulia by (*25*).
4. Materials and methods are available as supporting material on *Science* Online.
5. S. Hudson, *Remote Sens. Rev.* **8**, 195 (1993).
6. Beta-Alpha delay-Doppler differences from our 1 and 2 June 2002 observations are fit acceptably well by an orbit estimated from just the May 2001 observations if we allow for a 189° adjustment to the 2002 orbital phase.
7. The Arecibo delay residuals reveal a systematic bias possibly involving a several-decameter error in the nominal geodetic location of the telescope's reference point. The Goldstone astrometric measurements seem free from such a bias and provide much better orbital-phase coverage and twice the time base of the Arecibo astrometry.
8. D. J. Scheeres, *Icarus* **110**, 225 (1994).
9. R. P. Binzel *et al.*, *Icarus* **170**, 259 (2004).
10. G. J. Consolmagno, D. T. Britt, C. P. Stoll, *Meteorit. Planet. Sci.* **33**, 1221 (1998).
11. J. Wasson, in *Meteorites* (Springer, New York, 1974), pp. 175–176.
12. S. Abe *et al.*, *Science* **312**, 1344 (2006).
13. D. K. Yeomans *et al.*, *Science* **289**, 2085 (2000).
14. M. J. S. Belton *et al.*, *Nature* **374**, 785 (1995).
15. D. K. Yeomans *et al.*, *Science* **278**, 2106 (1997).
16. D. T. Britt, D. Yeomans, K. Housen, G. Consolmagno, in *Asteroids III*, W. Bottke, A. Cellino, P. Paolicchi, R. P. Binzel, Eds. (Univ. of Arizona, Tucson, AZ, 2002), pp. 485–500.
17. E. Asphaug, W. Benz, *Icarus* **121**, 225 (1996).
18. W. F. Bottke, H. J. Melosh, *Nature* **381**, 51 (1996).
19. D. C. Richardson, W. F. Bottke, S. G. Love, *Icarus* **134**, 47 (1998).
20. D. C. Richardson, K. J. Walsh, *Annu. Rev. Earth Planet. Sci.* **34**, 47 (2006).
21. D. P. Rubincam, *Icarus* **148**, 2 (2000).
22. D. J. Scheeres *et al.*, *Science* **314**, 1280 (2006); published online 12 October 2006 (10.1126/science.1133599).
23. A. Milani, Near-Earth Objects Dynamic Site: (66391) 1999KW4—Proper elements and encounter conditions (2006); available online at http://newton.dm.unipi.it/cgi-bin/neodys/neoibo?objects:1999KW4;properel;gif.
24. G. F. Gronchi, A. Milani, *Icarus* **152**, 58 (2001).
25. C. Magri *et al.*, *Icarus*, in press.
26. The radar predictions for the Sun-Earth-Alpha-Beta geometry at the photometric mutual event epochs establish that all the mutual events observed in June were eclipses (of Alpha on 3, 6, and 11 June and of Beta on 7 and 12 June).
27. D. J. Finney, in *Statistical Method in Biological Assay* (Hafner, New York, ed. 2, 1964), p. 24.
28. S. J. Ostro *et al.*, *J. Geophys. Res.* **97**, 18227 (1992).
29. http://reason.jpl.nasa.gov/~ostro/kw4/index.html

30. We thank the technical staffs of the Arecibo Observatory and the Goldstone Solar System Radar for help with the observations. Some of this work was performed at the Jet Propulsion Laboratory (JPL), California Institute of Technology, under contract with NASA. This material is based in part on work supported by NASA under the Science Mission Directorate Research and Analysis Programs. The Arecibo Observatory is part of the National Astronomy and Ionosphere Center, which is operated by Cornell University under a cooperative agreement with the NSF. Research at the University of Michigan was supported by NASA's Planetary Geology and Geophysics Program, by the JPL/Caltech Director's Research and Development Fund, and by the Air Force Office of Scientific Research. J.L.M. was supported in part by NASA grant NNG04GN31G. C.M. was partially supported by NSF grant AST-0205975. The work at Ondřejov was supported by the Grant Agency of the Czech Republic (grant 205/05/0604).

Supporting Online Material

www.sciencemag.org/cgi/content/full/1133622/DC1
Methods
Figs. S1 to S4
Tables S1 to S4
References

8 August 2006; accepted 4 October 2006
Published online 12 October 2006;
10.1126/science.1133622
Include this information when citing this paper.

Dynamical Configuration of Binary Near-Earth Asteroid (66391) 1999 KW4

D. J. Scheeres,[1]* E. G. Fahnestock,[1] S. J. Ostro,[2] J.-L. Margot,[3] L. A. M. Benner,[2] S. B. Broschart,[1] J. Bellerose,[1] J. D. Giorgini,[2] M. C. Nolan,[4] C. Magri,[5] P. Pravec,[6] P. Scheirich,[6] R. Rose,[2] R. F. Jurgens,[2] E. M. De Jong,[2] S. Suzuki[2]

Dynamical simulations of the coupled rotational and orbital dynamics of binary near-Earth asteroid 66391 (1999 KW4) suggest that it is excited as a result of perturbations from the Sun during perihelion passages. Excitation of the mutual orbit will stimulate complex fluctuations in the orbit and rotation of both components, inducing the attitude of the smaller component to have large variation within some orbits and to hardly vary within others. The primary's proximity to its rotational stability limit suggests an origin from spin-up and disruption of a loosely bound precursor within the past million years.

Binary systems in the near-Earth asteroid (NEA) population appear to be common (*1*). Because of their small sizes, binary NEAs' dynamical states and evolutionary histories may be very unlike those of other binaries in the solar system (the Earth-Moon and Pluto-Charon systems, large mainbelt asteroid binaries, and binary Kuiper Belt objects). Previous analyses of binary-system dynamics (*2*) have not considered situations with nonspherical components and strong coupling between translational and rotational motion. Radar images have characterized binary NEA (66391) 1999 KW4 in detail (*3*), and here we explore the full dynamics of the KW4 system with numerical simulations that solve the equations of motion for the coupled evolution of orbit and rotation.

Our simulations model the orbital dynamics as the relative motion between the body centers of mass and model the rotational dynamics using Euler's and attitude kinematic equations for each body (*4*). The system conserves total angular momentum and energy in the absence of external perturbations but may lose energy through internal dissipation. The coupled rotational and orbital dynamics are driven by the system's mutual gravitational potential, which is an explicit function of the relative position and attitude of the two bodies. The mutual potential between the radar-derived models of KW4's primary and secondary components (Alpha and Beta) are computed using a mutual potential expansion specialized for polyhedral models (*5*–*7*). Propagation of the system's dynamical evolution over several-month time scales has been made tractable by using a variational integrator (*8*) and a parallel computer with up to 256 processors (*9*).

Ostro *et al.* (*3*) find that the average relative orbit is nearly circular with a period of 17.4 hours and a separation of 2.54 km, that Beta's rotation is synchronous on average, and that Alpha's rotation pole and the binary orbit normal are separated by between 0 and 7.5°, with a nominal separation of 3.2°. Our simulations identify an energetically relaxed configuration for the coupled orbit and rotational dynamics, with the orbit and Alpha angular momentum vectors aligned, Beta rotating synchronously with small departures of its long axis from the Beta-Alpha line, and modest dynamical variations (Figs. 1 and 2). The eccentricity of the relaxed orbit, ~0.0113, is nonzero because of the

[1]Department of Aerospace Engineering, University of Michigan, 1320 Beal Avenue, Ann Arbor, MI 48109–2140, USA. [2]Jet Propulsion Laboratory, California Institute of Technology, 4800 Oak Grove Drive, Pasadena, CA 91109–8099, USA. [3]Department of Astronomy, Cornell University, 304 Space Sciences Building, Ithaca, NY 14853, USA. [4]Arecibo Observatory, HC03 Box 53995, Arecibo, Puerto Rico 00612, USA. [5]Department of Natural Sciences, University of Maine at Farmington, 173 High Street, Farmington, ME 04938, USA. [6]Astronomical Institute, Academy of Sciences of the Czech Republic Fričova 1, CZ-25165 Ondřejov, Czech Republic.

*To whom correspondence should be addressed. E-mail: scheeres@umich.edu